MODELING OF THE TEMPERATURE DISTRIBUTION OF A GREENHOUSE USING FINITE ELEMENT DIFFERENTIAL NEURAL NETWORKS

Juan Carlos Bello-Robles, Ofelia Begovich, Javier Ruiz-León and Rita Quetziquel Fuentes-Aguilar

Most of the existing works in the literature related to greenhouse modeling treat the temperature within a greenhouse as homogeneous. However, experimental data show that there exists a temperature spatial distribution within a greenhouse, and this gradient can produce different negative effects on the crop. Thus, the modeling of this distribution will allow to study the influence of particular climate conditions on the crop and to propose new temperature control schemes that take into account the spatial distribution of the temperature. In this work, a Finite Element Differential Neural Network (FE-DNN) is proposed to model a distributed parameter system with a measurable disturbance input. The learning laws for the FE-DNN are derived by means of Lyapunov's stability analysis and a bound for the identification error is obtained. The proposed neuro identifier is then employed to model the temperature distribution of a greenhouse prototype using data measured inside the greenhouse, and showing good results.

Keywords: differential neural networks, distributed parameter systems, greenhouse temperature modeling

Classification: 93C95, 93C20

1. INTRODUCTION

A greenhouse is a structure designed to create a microclimate that allows an adequate growth of the crop and isolates it from adverse external conditions. In this sense, climate control schemes have been created to provide a favorable environment inside the greenhouse, improving the development of the crop and reducing the water supply and energy consumption. In order to develop a climate control scheme for a greenhouse, it is necessary to obtain a mathematical model which describes accurately enough the dynamic behavior of the climate variables.

Numerous works have handled this modeling problem, assuming that the temperature is uniformly distributed within the greenhouse [7, 9, 12, 14]. However, experimental data show that there exists a temperature gradient within the greenhouse; this gradient can produce different negative effects on the crop, like plague generation, a decrease in

growth, early aging, etc. [2, 6], then a model that captures these temperature variations due to the spatial distribution is necessary. Systems that exhibit temporal and spatial distribution are called Distributed Parameter Systems (DPS) and are described by Partial Differential Equations (PDEs), and these equations can model different physical phenomena like diffusion process, wave propagation, and potential fields, among others [15]. In general, the greenhouse dynamics are nonlinear, coupled and with external disturbances, such as solar radiation, external air temperature, and humidity. Since the greenhouse temperature gradient follows a heat diffusion dynamics, it can be modeled by PDEs, but obtaining an analytic solution for PDEs is a difficult task, and not always possible to solve [5]. One way to overcome this problem is by using a numerical method to approximate a solution to these equations. But in this case it is necessary to know all the parameters of the PDEs that describe the system, which are not always available. When not all the parameters of the system are known or there is uncertainty in the mathematical description, Differential Neural Networks (DNN) could be used to obtain a nonparametric model, with additional advantages like dealing with disturbances and unmodeled dynamics [8, 11]. Indeed, DNNs have found a wide range of applications in different fields, and fundamental properties like stability and time delays have been deeply investigated [13, 16, 17]. Moreover, the facility to propose the number of layers and its neurons allows to incorporate different PDE discretization procedures in the neural network. For instance, in [3] a finite difference scheme is employed to discretize the spatial partial derivatives of certain PDEs obtaining a set of Ordinary Differential Equations (ODEs), and then each ODE that corresponds to a node of the constructed mesh is approximated by a DNN. Also in [1], the Finite Element Method (FEM) is employed to discretize the domain of certain PDEs, where the stiffness matrix defines the hidden layer weight of the neural network, called Finite Element Differential Neural Networks (FE-DNN). However the network considered in this reference is only for an autonomous PDE, so no input is considered.

The main contributions of the present work are the following. First, we extend the results from [1], considering also the presence of an input in the PDE. Thus, an FE-DNN is proposed to identify the dynamics of a DPS with a measurable disturbance input, where the learning laws for the FE-DNN are derived using Lyapunov stability analysis and a bound for the identification error is obtained. Then, the FE-DNN is used to model the greenhouse temperature using data measured at different points inside the greenhouse, and considering the solar radiation as disturbance input. As shown in the simulation results, the proposed FE-DNN achieves well the identification of the temperature distribution of the greenhouse prototype, obtaining a good performance in terms of the Total Mean Square Error (TMSE).

The organization of this work is as follows. In Section 2, the representation of the greenhouse temperature dynamics as a DPS and its approximation by means of an FE-DNN is introduced. In Section 3, the description of the neural network structure and the learning laws are presented. The experimental setup, which includes the physical characteristics of the greenhouse prototype is described in Section 4. Section 5 shows the obtained results, where different parameters of the FE-DNN were tested to obtain a desired TMSE. Finally, we end with some conclusions.

2. PROBLEM FORMULATION

In order to study the temperature spatial distribution, we will consider in this work a greenhouse prototype as a distributed parameter system whose temperature dynamics are described by a 2D parabolic PDE:

$$u_t = f(u_{xx}, u_{yy}, u_{xy}, u_x, u_y, u) + r + \xi \tag{1}$$

where $u = u(x, y, t) \in \Re$ is the temperature at the point (x, y) at time t defined in a domain $x \in [0, a]$, $y \in [0, b]$, time $t \geq 0$, and $u_t := \frac{\partial u}{\partial t}$, $u_x := \frac{\partial u}{\partial x}$, $u_{xx} := \frac{\partial^2 u}{\partial x^2}$, $u_y := \frac{\partial u}{\partial y}$, $u_{yy} := \frac{\partial^2 u}{\partial y^2}$, $u_{xy} := \frac{\partial^2 u}{\partial x \partial y}$; $r = r(x, y, t)$ is a measurable disturbance input to the system and $\xi = \xi(x, y, t)$ is considered as a nonmeasurable but bounded deterministic disturbance in the system.

Following the procedure described in [1], the Finite Element Method is applied to (1) and the next n ODEs are obtained:

$$\frac{\mathrm{d}u}{\mathrm{d}t} = g(x, y, t)u + h(r) + \xi \tag{2}$$

where $g(x, y, t)$ is the spatial discretization of Equation (1) given by the stiffness matrix of the spatial derivative terms and $h(r)$ is a function of the input. It is assumed that there exists a set of parameters

$$W_1^* \in \Re^{n \times n}, \ V_1^* \in \Re^{n \times n}, \ W_2^* \in \Re^{n \times n}, \ V_2^* \in \Re^{n \times n}$$

such that Equation (2) can be represented by the next differential neural network:

$$\frac{\mathrm{d}u}{\mathrm{d}t} = Au + W_1^* \sigma(V_1^* u) + W_2^* \varphi(V_2^* r) + \tilde{f} + \xi \tag{3}$$

where $u = u(x, y, t) \in \Re^n$ is the vector state of the system, $r = \Gamma r'$, where $\Gamma \in \Re^n$ is a vector of ones, r' is a measurable disturbance input, $A \in \Re^{n \times n}$ is a Hurtwitz matrix, and σ and φ are common sigmoid activation functions. The term $\tilde{f} = \tilde{f}(x, y, t)$ represents the modeling error defined as:

$$\tilde{f} = g(x, y, t)u + h(r) - [Au + W_1^* \sigma(V_1^* u) + W_2^* \varphi(V_2^* r)].$$

Additionally, the assumptions and properties for the DNN are the following [13]:

Assumption 1. The differences of the sigmoid function σ fulfill the generalized Lipschitz condition given by

$$\tilde{\sigma}^T \Lambda_1 \tilde{\sigma} \leq \Delta^T \Lambda_\sigma \Delta \tag{4}$$

where

$$\tilde{\sigma} := \sigma(V_1^* \hat{u}) - \sigma(V_1^* u)$$
$$\Delta := \hat{u} - u$$

and $\Lambda_1 \in \Re^{n \times n}$ and $\Lambda_\sigma \in \Re^{n \times n}$ are known as normalizing positive constants matrices.

Property 1. Because the sigmoid functions σ and φ are differentiable and satisfy the Lipschitz conditions, the next properties are satisfied:

$$\tilde{\sigma}' = \sigma(V_1\hat{u}) - \sigma(V_1^*\hat{u}) = D_\sigma \tilde{V}_1 \hat{u} + v_\sigma$$

$$D_\sigma = \left.\frac{\partial \sigma(Z)}{\partial Z}\right|_{Z=V_1\hat{u}} \in \Re^{m \times m}, \qquad \|v_\sigma\|_{\Lambda_1}^2 \leq l_1 \|\tilde{V}_1\hat{u}\|_{\Lambda_1}^2, \qquad l_1 > 0 \qquad (5)$$

$$\tilde{V}_1 = V_1 - V_1^*,$$

$$\tilde{\varphi}' := \varphi(V_2 r) - \varphi(V_2^* r) = D_\varphi \tilde{V}_2 r + v_\varphi$$

$$D_\varphi = \left.\frac{\partial \varphi(Z)}{\partial Z}\right|_{Z=V_2 r} \in \Re^{m \times m}, \qquad \|v_\sigma\|_{\Lambda_2}^2 \leq l_2 \|\tilde{V}_2 r\|_{\Lambda_2}^2, \qquad l_2 > 0 \qquad (6)$$

$$\tilde{V}_2 = V_2 - V_2^*.$$

Assumption 2. The unmodeled dynamics $\tilde{f}$ are bounded by

$$\|\tilde{f}\|_{\Lambda_{\tilde{f}}}^2 \leq \eta, \qquad \eta \in \Re^+. \qquad (7)$$

Assumption 3. The deterministic disturbance ξ is bounded by

$$\|\xi\|_{\Lambda_\xi}^2 \leq \gamma, \qquad \gamma \in \Re^+. \qquad (8)$$

Assumption 4. For a given matrix A there exist strictly positive definite matrices P and Q such that the next LMI problem:

$$\begin{bmatrix} -PA - A^T P - Q & P \\ P & R^{-1} \end{bmatrix} > 0 \qquad (9)$$

has a solution, where

$$R = 2\bar{W}_1 + \bar{W}_2 + \Lambda_{\tilde{f}}^{-1} + \Lambda_\xi^{-1}$$
$$\bar{W}_1 = W_1^* \Lambda_1^{-1} W_1^{*T}$$
$$\bar{W}_2 = W_2^* \Lambda_1^{-1} W_2^{*T}$$
$$Q = Q_0 + \Lambda_\sigma$$

and $\Lambda_{\tilde{f}}$, Λ_ξ, and Q_0 are predefined positive definite matrices.

Considering the definitions and properties presented above, now we can state the first problem to be tackled in this work: to propose a neural representation of the form (3) for the DPS (1), with the hidden layer V_1 containing the nodal interconnection structure provided by the stiffness matrix, to establish the learning laws and an upper bound for the identification error:

$$\mu := \lim_{t \to \infty} \|\hat{u}(t) - u(t)\|^2, \qquad (10)$$

and to find parameters participating in the FE-DNN structure in order to reduce μ to its lowest achievable value. Then this FE-DNN along with the learning laws will be used to model the temperature dynamics of a greenhouse.

3. FINITE ELEMENT NEURAL NETWORK IDENTIFICATION

3.1. Differential neural network structure

Following the methodology described in [1], but considering the presence of a measurable disturbance input, the next FE-DNN identifier is proposed:

$$\frac{d\hat{u}}{dt} = A\hat{u} + W_1\sigma(V_1\hat{u}) + W_2\varphi(V_2 r) \tag{11}$$

where $\hat{u} = \hat{u}(x, y, t) \in \Re^n$ is the estimated state of the system, σ and φ are sigmoid activation functions, $r = \Gamma r'$, where $\Gamma \in \Re^n$ is a vector of ones, r' is a measurable disturbance input, $A \in \Re^{n \times n}$ is a Hurtwitz matrix, $W_1 = W_1(t)$, $W_2 = W_2(t) \in \Re^{n \times n}$ are output weight matrices and $V_1 = V_1(t)$, $V_2 = V_2(t) \in \Re^{n \times n}$ are hidden layer weight matrices, where the hidden layer V_1 takes the structure of the stiffness matrix K, i.e., where the stiffness matrix elements are zero, the elements of the hidden layer are zero too.

3.2. Learning laws for the neuro identifier weights

The weight matrices in Equation (11) are updated by the next learning laws:

$$\begin{aligned}
\dot{W}_1 &= -k_1 P\Delta\sigma^T + k_1 P\Delta\hat{u}^T \tilde{V}_1^T D_\sigma^T - \beta\tilde{W}_1 \\
\dot{V}_1 &= -k_2 D_\sigma^T W_1^T P\Delta\hat{u}^T - \frac{k_2 l_1}{2}\Lambda_1 \tilde{V}_1 \hat{u}\hat{u}^T - \beta\tilde{V}_1 \\
\dot{W}_2 &= -k_3 P\Delta\varphi^T + k_3 P\Delta r^T \tilde{V}_2^T D_\varphi^T - \beta\tilde{W}_2 \\
\dot{V}_2 &= -k_4 D_\varphi^T W_2^T P\Delta r^T - \frac{k_4 l_2}{2}\Lambda_2 \tilde{V}_2 r r^T - \beta\tilde{V}_2
\end{aligned} \tag{12}$$

where k_i, $i = 1, \ldots, 4$ and $\beta \in \Re$ are positive real numbers, P is the solution of Equation (9) and $\tilde{W}_i = W_i - W_i^*$, $i = 1, 2$.

3.3. Identification error stability analysis

In this section, we show that the proposed neuro-identifier ensures a bound in the identification error of a distributed parameter system under the action of a measurable disturbance input.

Consider the perturbed distributed parameter system described by the PDE (1) and approximated by the FEM in Equation (2). It is assumed that it is possible to have discrete measurements in a finite number of points on the domain, called nodes. The measured data define the system state $u(t)$ and the number of nodes defines the dimension of the state vector. Also, consider that the system is under the action of a measurable disturbance input $r(t)$.

Theorem 3.1. If the Assumptions $1-4$ are satisfied and the weight matrices W_1, V_1, W_2 and V_2 of the FE-DNN (11) are adjusted by the learning laws (12), then the identification error and the weights are bounded, i.e., $(\Delta, W_1, V_1, W_2, V_2) \in L_\infty$, and the norm of the identification error converges exponentially to a bounded region given by

$$\lim_{t \to \infty} \|\Delta\|_2 \leq \sqrt{\frac{\eta + \gamma}{\beta\lambda_{\min}(P)}}. \tag{13}$$

P r o o f.   Let us define the identification error as:

$$\Delta = \hat{u} - u. \tag{14}$$

Thus, from (3) and (11), the derivative of the error is given by

$$\dot{\Delta} = A\Delta + \tilde{W}_1\sigma(V_1\hat{u}) + W_1^*\tilde{\sigma} + W_1^*\tilde{\sigma}' + \tilde{W}_2\varphi(V_2r) + W_2\tilde{\varphi}' - \tilde{f} - \xi. \tag{15}$$

Consider the Lyapunov-like function defined as:

$$V = \Delta P\Delta + tr\{\tilde{W}_1^T k_1^{-1}\tilde{W}_1\} + tr\{\tilde{V}_1^T k_2^{-1}\tilde{V}_1\} + tr\{\tilde{W}_2^T k_3^{-1}\tilde{W}_2\} + tr\{\tilde{V}_2^T k_4^{-1}\tilde{V}_2\}. \tag{16}$$

Taking its derivative we get

$$\dot{V} = 2\Delta^T P\dot{\Delta} + 2tr\{\tilde{W}_1^T k_1^{-1}\dot{W}_1\} + 2tr\{\tilde{V}_1^T k_2^{-1}\dot{V}_1\} + 2tr\{\tilde{W}_2^T k_3^{-1}\dot{W}_2\} + 2tr\{\tilde{V}_2^T k_4^{-1}\dot{V}_2\}. \tag{17}$$

Using Equation (15) in the first term of (17), we have

$$\begin{aligned} 2\Delta^T P\dot{\Delta} =& 2\Delta^T PA\Delta + 2\Delta^T P\tilde{W}_1\sigma(V_1\hat{u}) + 2\Delta^T P\tilde{W}_2\varphi(V_2r) + 2\Delta^T PW_1^*\tilde{\sigma} \\ & + 2\Delta^T PW_1^*\tilde{\sigma}' + 2\Delta^T PW_2^*\tilde{\varphi}' - 2\Delta^T P\tilde{f} - 2\Delta^T P\xi. \end{aligned}$$

Using the matrix lambda inequality: $X^T Y + Y^T X \leq X^T \Lambda X + Y^T \Lambda^{-1} Y$, proved in [13], the Assumptions 1-3 and the Property 1 in the last five terms of the equation above, we get the following inequalities:

$$\begin{aligned} 2\Delta^T PW_1^*\tilde{\sigma} &\leq \Delta^T PW_1^*\Lambda_1^{-1}W_1^{*T}P\Delta + \tilde{\sigma}^T\Lambda_1\tilde{\sigma} \\ &\leq \Delta P\bar{W}_1 P\Delta + \Delta^T\Lambda_\sigma\Delta, \end{aligned}$$

$$\begin{aligned} 2\Delta^T PW_1^*\tilde{\sigma}' &= 2\Delta^T PW_1^* D_\sigma\tilde{V}_1\hat{u} + 2\Delta^T PW_1^* v_\sigma \\ &\leq 2\Delta^T PW_1 D_\sigma\tilde{V}_1\hat{u} - 2\Delta^T P\tilde{W}_1 D_\sigma\tilde{V}_1\hat{u} + \Delta^T P\bar{W}_1 P\Delta + l_1\|\tilde{V}_1\hat{u}\|^2_{\Lambda_1}, \end{aligned}$$

$$\begin{aligned} 2\Delta^T PW_2^*\tilde{\varphi}' &= 2\Delta^T PW_2^* D_\varphi\tilde{V}_2 r + 2\Delta^T PW_2^* v_\varphi \\ &\leq 2\Delta^T PW_2 D_\varphi\tilde{V}_2 r - 2\Delta^T P\tilde{W}_2 D_\varphi\tilde{V}_2 r + \Delta^T P\bar{W}_2 P\Delta + l_2\|\tilde{V}_2 r\|^2_{\Lambda_2}, \end{aligned}$$

$$-2\Delta^T P\tilde{f} \leq \Delta P\Lambda_{\tilde{f}}^{-1}P\Delta + \tilde{f}^T\Lambda_{\tilde{f}}\tilde{f},$$
$$-2\Delta^T P\xi \leq \Delta^T P\Lambda_\xi^{-1}P\Delta + \xi^T\Lambda_\xi\xi.$$

So, using the above inequalities, the Equation (17) takes the form

$$\begin{aligned}
\dot{V} \leq{} & \Delta^T(PA + A^TP + P(2\bar{W}_1 + \bar{W}_2 + \Lambda_{\tilde{\xi}}^{-1} + \Lambda_{\tilde{f}}^{-1})P + \Lambda_\sigma)\Delta \\
& + 2\Delta^TP\tilde{W}_1\sigma - 2\Delta^TP\tilde{W}_1D_\sigma\tilde{V}_1\hat{u} + \frac{1}{k_1}tr\{\tilde{W}_1^T\dot{W}_1\} + \frac{\beta}{k_1}tr\{\tilde{W}_1^T\tilde{W}_1\} \\
& + 2\Delta^TPW_1D_\sigma\tilde{V}_1\hat{u} + l_1\hat{u}^T\tilde{V}_1^T\Lambda_1\tilde{V}_1\hat{u} + \frac{1}{k_2}tr\{\tilde{V}_1^T\dot{V}_1\} + \frac{\beta}{k_2}tr\{\tilde{V}_1^T\tilde{V}_1\} \\
& + 2\Delta^TP\tilde{W}_2\varphi - 2\Delta^TP\tilde{W}_2D_\varphi\tilde{V}_2r + \frac{1}{k_3}tr\{\tilde{W}_2^T\dot{W}_2\} + \frac{\beta}{k_3}tr\{\tilde{W}_2^T\tilde{W}_2\} \\
& + 2\Delta^TPW_2D_\varphi\tilde{V}_2r + l_2r^T\tilde{V}_2^T\Lambda_2\tilde{V}_2r + \frac{1}{k_4}tr\{\tilde{V}_2^T\dot{V}_2\} + \frac{\beta}{k_4}tr\{\tilde{V}_2^T\tilde{V}_2\} \\
& - \frac{\beta}{k_1}tr\{\tilde{W}_1^T\tilde{W}_1\} - \frac{\beta}{k_2}tr\{\tilde{V}_1^T\tilde{V}_1\} - \frac{\beta}{k_3}tr\{\tilde{W}_2^T\tilde{W}_2\} - \frac{\beta}{k_4}tr\{\tilde{V}_2^T\tilde{V}_2\} + \eta + \gamma.
\end{aligned}$$

Using Assumption 4 and the learning laws (12) in the inequality above, we have

$$\begin{aligned}
\dot{V} \leq{} & -\Delta^TP^{1/2}(P^{-1/2}Q_0P^{-1/2})P^{1/2}\Delta - \frac{\beta}{k_1}tr\{\tilde{W}_1^T\tilde{W}_1\} - \frac{\beta}{k_2}tr\{\tilde{V}_1^T\tilde{V}_1\} - \frac{\beta}{k_3}tr\{\tilde{W}_2^T\tilde{W}_2\} \\
& - \frac{\beta}{k_4}tr\{\tilde{V}_2^T\tilde{V}_2\} + \eta + \gamma.
\end{aligned}$$

Choosing $\beta = \lambda_{\min}(P^{-1/2}Q_0P^{-1/2})$, then

$$\begin{aligned}
\dot{V} \leq{} & -\beta\big(\Delta^TP\Delta + tr\{\tilde{W}_1k_1^{-1}\tilde{W}_1\} + tr\{\tilde{V}_1k_1^{-1}\tilde{V}_1\} + tr\{\tilde{W}_2k_3^{-1}\tilde{W}_2\} + tr\{\tilde{V}_2k_4^{-1}\tilde{V}_2\}\big) + \eta + \gamma \\
\leq{} & -\beta V + \Psi,
\end{aligned}$$

where $\Psi := \eta + \gamma$.

Solving the last inequality, we have

$$V \leq e^{-\beta t}V_0 + \frac{\Psi}{\beta}(1 - e^{-\beta t}). \tag{18}$$

From Equation (16) and using Rayleigh's inequality we have

$$\lambda_{\min}(P)\Delta^T\Delta \leq V. \tag{19}$$

Inequalities (18) and (19) imply that

$$\|\Delta\|_2 \leq \sqrt{\frac{e^{-\beta t}V_0 + \frac{\Psi}{\beta}(1 - e^{-\beta t})}{\lambda_{\min}(P)}}. \tag{20}$$

Finally, taking the limit $t \to \infty$ on the last inequality, the bound of the identification error (13) is obtained. $\qquad\square$

4. EXPERIMENTAL SETUP

In this section, we present the main characteristics of the greenhouse prototype that is considered in this research, including description, dimensions, sensors layout and the data acquisition.

4.1. Experimental prototype

The experimental greenhouse prototype used in this work is located at Cinvestav Campus Guadalajara in Zapopan, Jalisco, Mexico (20°40'06.7"N, 103°27'54.1"W). The greenhouse is 12 m long, 5 m wide, and 5.14 m of maximal height. The greenhouse is equipped with:

- A metallic structure cover with a plastic film, with 70 percent of transmittance

- 12 internal temperature sensors (°C)

- Internal and external relative humidity sensors (%)

- Internal and external wind speed sensors (m/s)

- Internal solar radiation sensor (W/m^2)

- Two fans of 1/4 HP and 750 m^3/h each one

- An Arduino MEGA 2560 as data acquisition device

- A computer with an Intel Core i7-2600K 3.4 GHz processor, 15.7 GB RAM DDR3 833 MHz and Windows 10 operative system

The four principal views and dimensions in meters of the prototype are shown in Figure 1.

4.1.1. Temperature sensors

The temperature inside the greenhouse prototype was measured and collected at different locations using 12 temperature sensors (LM35D Texas instruments, u_{11}-u_{43}) distributed as shown in Figure 2. The LM35D temperature sensor was chosen because of its easy implementation and technical specifications, in concrete his operating temperature range (see Table 1).

Temperature Sensor LM35D	
Operating temperature	0-100 °C
Supply Voltage	4-30 V
Current consumption at 5 V	40-80 (typ 56) μA
Accuracy at 25 °C	± 0.6 °C

Tab. 1. LM35D temperature sensor specifications.

The LM35D output voltage is given by

$$V_{out} = H \cdot T_{in} \tag{21}$$

where

$$H = 10 \text{ mV/°C} \tag{22}$$

is the LM35D transfer function and T_{in} is the temperature input in °C.

a) Top view   b) Isometric view

c) Front view   d) Side view
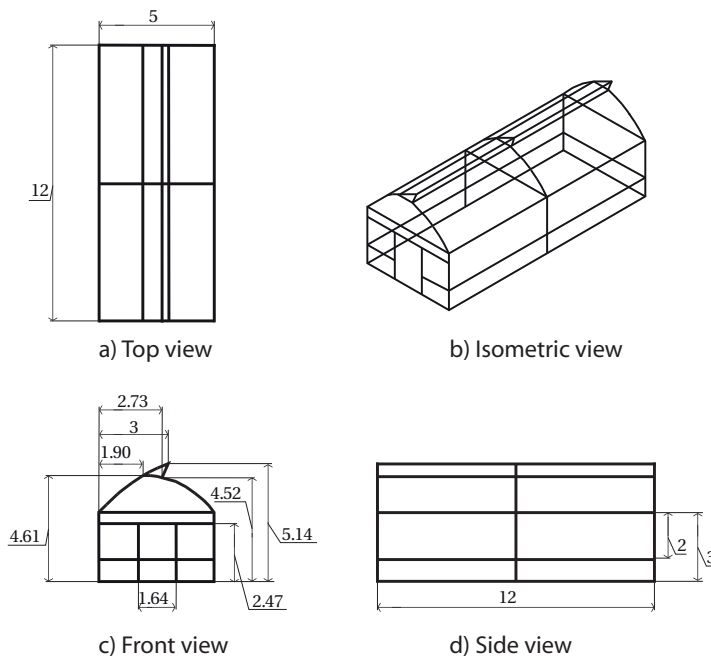
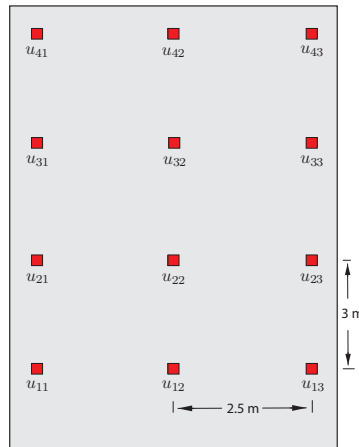**Fig. 1.** Greenhouse dimensions diagram.

Fig. 2. Greenhouse temperature sensors layout.

4.2. Data acquisition

The temperature inside the greenhouse prototype was measured and collected at different locations every 5 seconds using 12 temperature sensors. The experiment was conducted from 14:26 on July 25, 2017, to 14:26 on July 26, 2017. During the experimental period, no actuators were used and no crop was in the greenhouse. Figure 3 shows the measured temperature data at nodes u_{11}, u_{22} and u_{43} during all the experiment. It is important to point out that the temperature is not homogeneous within the greenhouse prototype, specially during the day when the solar radiation is present. This temperature distribution is one of the motivations to employ the identification scheme proposed in this work.
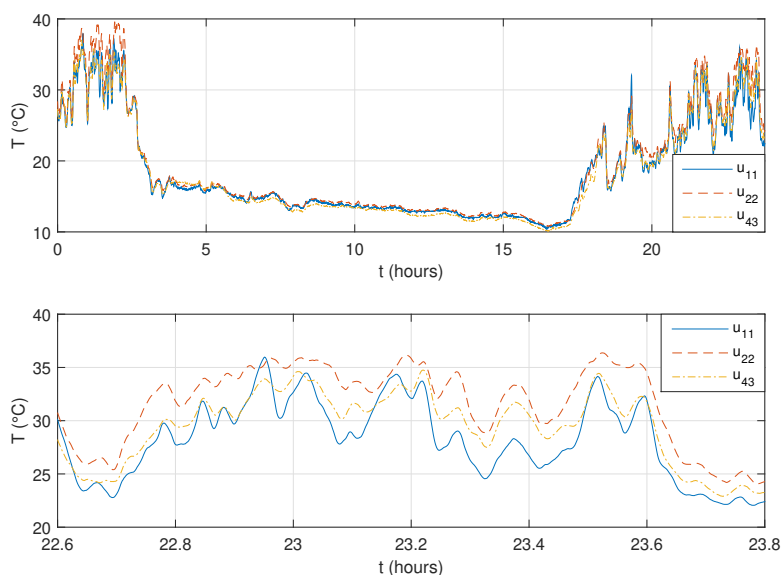

Fig. 3. Temperature data record at nodes u_{11}, u_{22} and u_{43}. (Top) during all the experiment. (Bottom) during an interval of 1.2 hours.

5. RESULTS

This section presents the design of the Finite Element Differential Neural Network and its implementation to model the temperature distribution of the greenhouse.

5.1. Temperature distribution identification

To perform the temperature distribution identification we consider the FE-DNN structure (11) and the learning laws (12) described in Section 3. The first step is to compute

the stiffness matrix where the following parameters were considered: $a = 5$, $b = 9$, $n = 12$, $n_x = 4$ and $n_y = 3$, where a is the length in the x direction and b the length in the y direction of the area occupied by the sensors, n the total number of nodes (temperature sensors), n_x is the number of nodes in the x direction and n_y the number of nodes in the y direction. The procedure to compute the stiffness matrix is well known, some references are [10] and [18]; the obtained stiffness matrix K is used as the mask of the hidden layer V_1 of the FE-DNN.

Next, the parameters for the neuro identifier are chosen by a trial and error procedure in such a way that the identification total mean square error (TMSE) is reduced to a value of 1×10^{-2}, the Table 2 shows the TMSE for different parameters of the FE-DNN. The mean square error (MSE) at time j is defined as:

$$\text{MSE}(j) = \frac{1}{N} \sum_{i=1}^{N} \left(\hat{u}_i(j) - u_i(j) \right)^2 \tag{23}$$

where N is the number of states of the DNN, $u_i(j)$ is the measured data and $\hat{u}(j)$ is the approximate data obtained with the FE-DNN at node i and at time j; the total mean square error (TMSE) is defined as:

$$\text{TMSE} = \frac{1}{M} \sum_{j=1}^{M} \text{MSE}(j) \tag{24}$$

where M is the total of sampled data.

The matrix $A = \lambda I_n$, with $\lambda = -0.6$ and the gains of the learning laws $k_1 = k_2 = 0.03$ and $k_3 = k_4 = 0.06$ were selected because the neuro-identifier achieves an acceptable identification error and presents a good transient response, the remaining parameters of the FE-DNN are the next:

$$V_1(0) = 0.01 V_1^*$$
$$W_1(0) = W_2(0) = V_2(0) = 0.01 M$$
$$\bar{W}_1 = W_1(0)^T W_1(0)$$
$$\bar{W}_2 = W_2(0)^T W_2(0)$$
$$\Lambda_1 = \Lambda_\sigma = \Lambda_f = \Lambda_\xi = Q_0 = I$$
$$\beta = 1.3637$$
$$\sigma = \frac{1}{1 + e^{(-0.05 V_1 \hat{u})}} + 0.005$$
$$\varphi = \frac{1}{1 + e^{(-0.01 V_2 r)}} + 0.001$$

where M is a matrix of ones of dimension $n \times n$, and P can be computed solving (9) with the above parameters. The systems of ODEs in the FE-DNN (11) and the learning laws (12) were solved in Simulink using the Bogacki-Shampine method with a fixed time step of 5 s. Figure 4 shows the performance of the neuro-identifier at the nodes u_{11}, u_{22} and u_{43} during the first 100 s, where it is possible to notice that at time $t = 40$ s

λ	k_1	k_3	TMSE
-0.6	0.030	0.04	0.0774
-0.6	0.035	0.04	0.0739
-0.6	0.040	0.04	0.0716
-0.6	0.030	0.05	0.0721
-0.6	0.035	0.05	0.0705
-0.6	0.040	0.05	0.0704
-0.6	0.030	0.06	0.0703
-0.6	0.035	0.06	0.0723
-0.6	0.040	0.06	0.0875

Tab. 2. Comparison of the total mean square error with different
DNN parameters.

the FE-DNN dynamics are almost the same as the greenhouse temperature dynamics. Figure 5 shows the performance of the neuro-identifier at nodes u_{11}, u_{22} and u_{43} during 2.5 hours (17 to 19.5 hours).
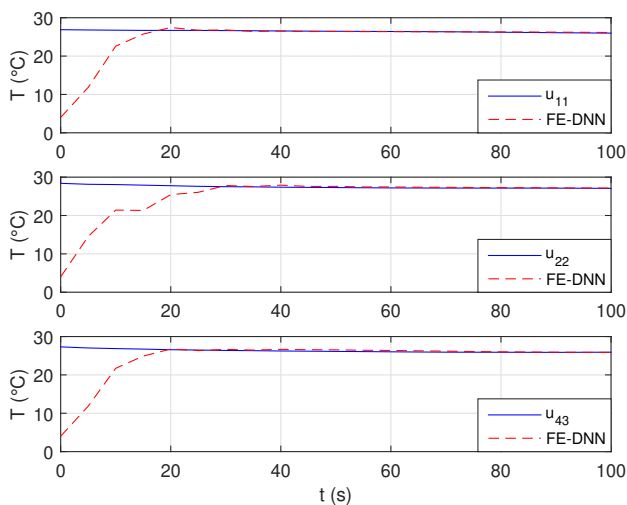

Fig. 4. Comparison of the measured data against the estimated data
at 3 temperature nodes during the first 100 s.

Figure 6 shows the normalized MSE plotted against time. The total mean square error throughout the duration of the experiment is computed, obtaining a value of **TMSE=0.0703**.   Figure 7 shows the temperature distribution measured at the 12 nodes $u_{11} - u_{43}$ and the respectively FE-DNN approximation of the temperature distribution $\hat{u}_{11} - \hat{u}_{43}$ at different times.
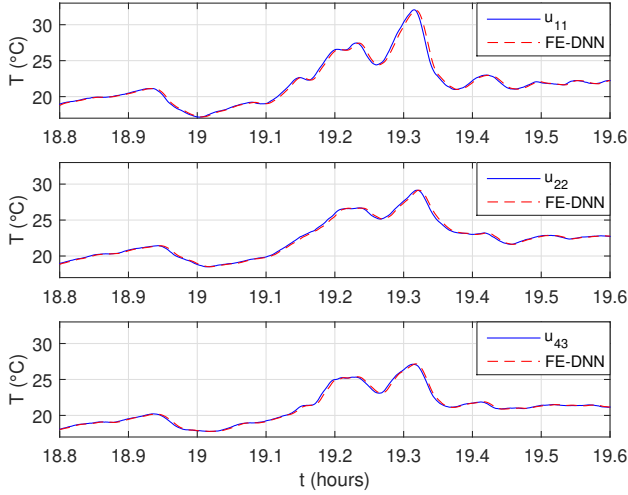
Fig. 5. Comparison of the measured data against the estimated data
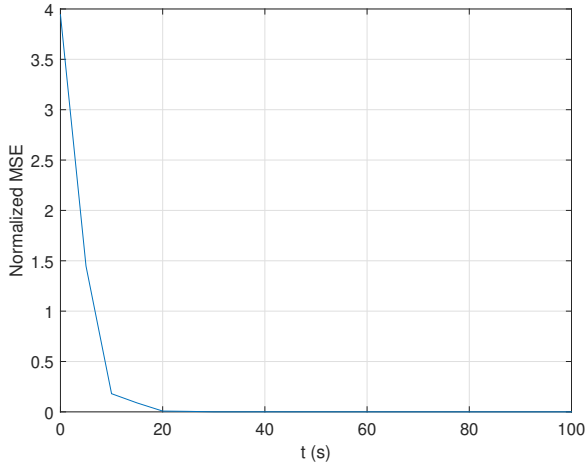at 3 temperature nodes during 2.5 hours.

Fig. 6. Normalized mean square error during the first 100 s.

Remark 1. The advantages of using the DNN based on the finite element method instead of the finite difference procedure is that only one DNN is needed to identify all the nodes, also the sparse structure of the hidden layer reduces its number of neurons, this results in a faster computation of the learning laws and the FE-DNN.
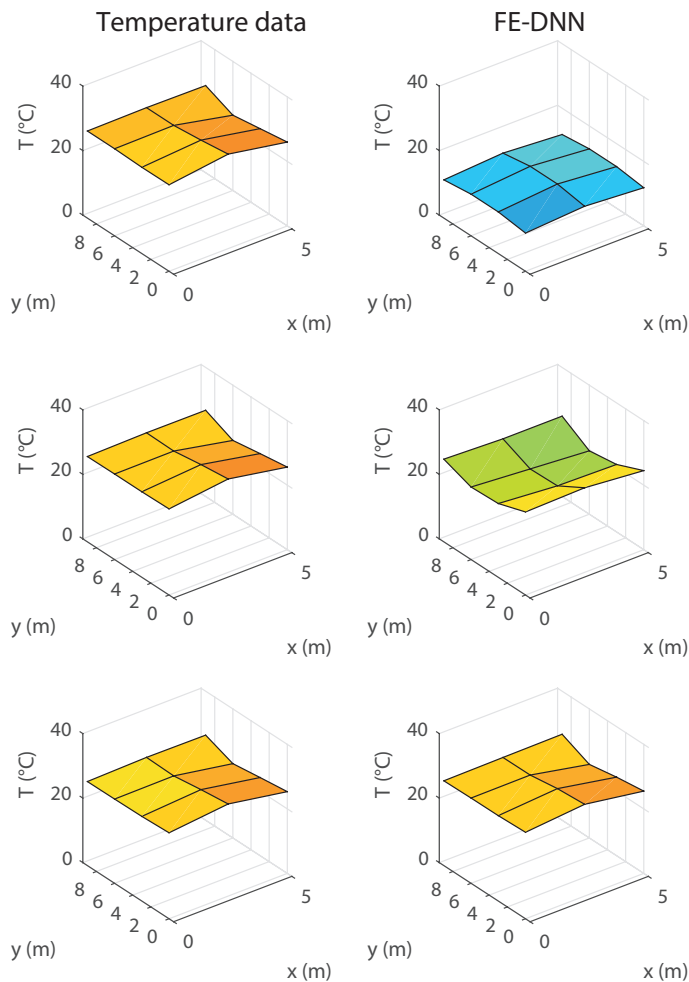
Fig. 7. Temperature distribution measured data in the left and
FE-DNN estimated data in the right at (Top) t=10 s, (Middle) t=20 s
and (Bottom) t=35 s.

Remark 2. Once that the identification problem is solved, the control stage can be
designed, where the actuator position can be chosen selecting a node as a control input
and studying the influence of this node in the system, an extra weight for the control
input is then necessary for the FE-DNN structure.

6. CONCLUSIONS

In this paper, the representation of a greenhouse temperature dynamics as a distributed parameter system was carried out by means of an FE-DNN that performs a nonparametric identification of the temperature distribution of a greenhouse prototype. The FEM was employed to discretize the greenhouse area into 12 nodes defined as the DNN states. The learning laws for the proposed FE-DNN were obtained by means of Lyapunov's second method and a bound for the identification error was obtained. The neuro identifier shows good results in terms of the TMSE.

For the greenhouse modeling there always exist dynamics that are not considered because it makes the model too complex or because they are unknown, also the external perturbations affecting the greenhouse produce that dynamics from mathematical models have deviations from measured data, in this context the differential neural networks are an appropriate solution to model the greenhouse dynamics. Moreover, due to the slow dynamics of the greenhouse temperature, it is possible to execute this neuro-identifier in real time.

As a future work, we shall increase the dimension of the state of the FE-DNN to include the internal humidity distribution dynamics of the greenhouse in the neural model.

REFERENCES

[1] O. Aguilar-Leal, R.Q. Fuentes, I. Chairez, A. Garcia, and J.C. Huegel: Distributed parameter system identification using finite element differential neural networks. Applied Soft Computing *43* (2016), 663–642. DOI:10.1016/j.asoc.2016.01.004

[2] A. Baille, C. Kittas, and N. Katsoulas: Influence of whitening on greenhouse microclimate and crop energy partitioning. Agricultural Forest Meteorology *107* (2001), 4, 293–306. DOI:10.1016/s0168-1923(01)00216-7

[3] I. Chairez, R. Fuentes, A. Poznyak, T. Poznyak, M. Escudero, and L. Viana: DNN-state identification of 2D distributed parameter systems. Int. J. Systems Sci. *43* (2012), 2, 296–307. DOI:10.1080/00207721.2010.495187

[4] J. Chen, Y. Cai, F. Xu, H. Hu, and Q. Ai: Analysis and optimization of the fan-pad evaporative cooling system for greenhouse based on CFD. Advances Mechanical Engrg. *6* (2014), 712–740. DOI:10.1155/2014/712740

[5] L.C. Evans: Partial Differential Equations. American Mathematical Soc., 2010.

[6] J. Fargues, N. Smits, M. Rougier, T. Boulard, G. Ridray, J. Lagier, B. Jeannequin, H. Fatnassi, and M. Mermier: Effect of microclimate heterogeneity and ventilation system on entomopathogenic hyphomycete infection of Trialeurodes vaporariorum (Homoptera: Aleyrodidae) in Mediterranean greenhouse tomato. Biolog. Control *32* (2005), 3, 461–472. DOI:10.1016/j.biocontrol.2004.12.008

[7] P.M. Ferreira, E.A. Faria, and A.E. Ruano: Neural network models in greenhouse air temperature prediction. Neurocomputing *43* (2002), 1, 51–75. DOI:10.1016/s0925-2312(01)00620-8

[8] R. Fuentes, A. Poznyak, I. Chairez, M. Franco, and T. Poznyak: Continuous neural networks applied to identify a class of uncertain parabolic partial differential equations. Int. J. Model. Simul. Sci. Comput. *1* (2010), 4, 485–508. DOI:10.1142/s1793962310000304

[9] A. Hasni, R. Taibi, B. Draoui, and T. Boulard: Optimization of greenhouse climate model parameters using particle swarm optimization and genetic algorithms. Energy Procedia *6* (2011), 371–380. DOI:10.1016/j.egypro.2011.05.043

[10] Y. W. Kwon and H. Bang: The Finite Element Method Using MATLAB. CRC Press, 2000. DOI:10.1201/9781315275949

[11] J. H. Perez-Cruz, A. Alanis, J. Rubio, and J. Pacheco: System identification using multilayer differential neural networks: a new result. J. Appl. Math. *2012* (2012), 1–20. DOI:10.1155/2012/529176

[12] A. Perez-Gonzalez, O. Begovich, and J. Ruiz-León: Modeling of a greenhouse prototype using PSO algorithm based on a LabView TM application. In: Proc. 2014 International Conference on Electrical Engineering, Computing Science and Automatic Control 1–6.

[13] A. S. Poznyak, E. N. Sanchez and Y. Wen: Differential Neural Networks for Robust Nonlinear Control: Identification, State Estimation and Trajectory Tracking. World Scientific, 2001. DOI:10.1142/4703

[14] P. Salgado and J. B. Cunha: Greenhouse climate hierarchical fuzzy modelling. Control Engrg. Practice *13* (2005), 5, 613–628. DOI:10.1016/j.conengprac.2004.05.007

[15] W. A. Strauss: Partial Differential Equations: An Introduction. John Wiley and Sons Inc, 2007.

[16] X. M. Zhang and Q. L. Han: Global asymptotic stability for a class of generalized neural networks with interval time-varying delays. IEEE Trans. Neural Networks *22* (2011), 8, 1180–1192. DOI:10.1109/tnn.2011.2147331

[17] X. M. Zhang and Q. L. Han: State estimation for static neural networks with time-varying delays based on an improved reciprocally convex inequality. IEEE Trans. Neural Networks Learning Systems *29* (2018), 4, 1376–1381. DOI:10.1109/tnnls.2017.2661862

[18] O. C. Zienkiewicz, R. L. Taylor, and J. Z Zhu: The Finite Element Method: Its Basis and Fundamentals. Elsevier Butterworth-Heinemann, 2005.

Juan Carlos Bello-Robles, CINVESTAV Unidad Guadalajara, Av. del Bosque 1145, Col. El Bajío, Zapopan, 45010, Jalisco. México.
  e-mail: jcbello@gdl.cinvestav.mx

Ofelia Begovich, CINVESTAV Unidad Guadalajara, Av. del Bosque 1145, Col. El Bajío, Zapopan, Jalisco. México.
  e-mail: obegovi@gdl.cinvestav.mx

Javier Ruiz-León, CINVESTAV Unidad Guadalajara, Av. del Bosque 1145, Col. El Bajío, Zapopan, Jalisco. México.
  e-mail: jruiz@gdl.cinvestav.mx

Rita Quetziquel Fuentes-Aguilar, Tecnológico de Monterrey, Campus Guadalajara, Jalisco. México.
  e-mail: rita.fuentes@itesm.mx